2024-01-2764

On the investigation of car steady-state cornering equilibria and drifting

Giovanni Righetti, Elisabetta Binetti, Ricardo De Castro, Roberto Lot, Matteo Massaro, Basilio Lenzo
University of Padova, Padua, Italy - University of California at Merced, USA

ABSTRACT

This paper proposes a thorough investigation of steady-state cornering equilibria for cars. Besides equilibria corresponding to normal driving behaviour - herein denoted as stable-normal turn, drifting is attracting increasing attention. When discussing drifting, it is typically assumed that yaw rate and steering angle have opposite signs, i.e. the driver is countersteering, and the rear axle is saturated. Interestingly, another unstable equilibrium is possible, herein referred to as unstable-normal turn. In this work, an attempt to give a comprehensive definition of drift is made. An inverse model is proposed to compute the driver inputs needed to perform a steady-state turn for a given radius and sideslip angle. The mathematical meaning of all equilibria is explored by linearizing the system and analyzing eigenvalues and eigenvectors of the resulting state matrices.

INTRODUCTION

Steady-state cornering analysis give insightful information about the attitude of a vehicle when negotiating a given turn. Drifting is one of the operating modes that may emerge in steady-state cornering. Racing drivers exploit drifting to reduce lap time, especially in gravel tracks or roads [1]. It is also a behavior that might emerge during emergency vehicle maneuvers in roads with low-grip surface. Having a fundamental understanding of the vehicle dynamic response in drifting conditions is important to design advanced vehicle control systems [2]. The existence and instability of drift equilibria have been established by several authors, who presented different techniques to prevent or handle it. Different strategies correspond to different vehicle models, ranging from the simplest single-track model to more complex formulations based e.g. on double track models taking into account roll, pitch, load transfers etc. In general, to analyze drifting, it is important to consider non-linear tire characteristics [3, 4, 5]. Goh and Gerdes [6] present a controller for autonomous drifting with simultaneous path tracking in which the trajectory is treated as a sequence of unstable equilibrium points. The model implemented is a four-wheel model with steady-state weight transfer. Peterson et al. [7] implement a controller using a linearization of a single-track vehicle model to capture the necessary dynamics around a drift equilibrium point. Vignati et al. [8] develop a torque-vectoring control strategy to assist the driver in controlling the vehicle in drifting condition. This control strategy is implemented and simulated in Matlab/Simulink using a Formula SAE vehicle with two rear independent electric motors, modeled as a vehicle with 14 degrees of freedom. Milani et al. [9] utilize a four-wheel model to calculate the equilibria in planar motion. Their study investigates drifting equilibrium differences between rear-wheel-drive and four-wheel-drive vehicles (4WD). The type of equilibrium is assessed using the phase portrait approach and the existence of an alternative drifting equilibrium (referred to as secondary drifting point) for 4WD vehicles is suggested.
This work presents a comprehensive investigation of drifting equilibria for single-track vehicle models. We provide three main contributions:

- We investigate the possible ways (steady-state equilibria) to negotiate a given turn with a desired sideslip angle. Our analysis reveals the existence of limit cycles in the (velocity, yaw-rate, sideslip) space, providing important insights into the dynamic vehicle behavior in extreme driving conditions.
- We propose a new classification for the steady-state cornering motion of vehicle. This classification takes into account not only the stability properties of the equilibria points but also "countersteering" factors.

- We introduce a simple non-linear lateral tire model, which is able to well approximate the Fiala tire model. It allows to obtain analytical expressions of the state matrix of the linearized system near any equilibrium.

VEHICLE AND TIRE MODELS

In order to investigate the existence of drifting equilibria maintaining low model complexity, a nonlinear single-track model is used. It is one of the simplest planar models, but it has been shown to be capable of capturing important aspects of vehicle handling behavior [9, 10]. Moreover, several researches have demonstrated that the single track model is suitable for analysing highly nonlinear maneuvers, but still steady-state, such as drifting [11]. Neither lateral nor longitudinal load transfer is considered to maintain low complexity of the system and the characteristics of the axle are resumed by one tire for the front and one for the rear. Rolling and pitching motion of the chassis are not taken into account. The dynamics of the model can be described by the following equations of motion [12]:

$$\begin{aligned}\dot{V} = \frac{1}{m}[&F_{xf}\cos(\delta-\beta) - F_{yf}\sin(\delta-\beta) \\ &+ F_{xr}\cos(\beta) + F_{yr}\sin(\beta)]\end{aligned} \tag{1}$$

$$\begin{aligned}\dot{\beta} = \frac{1}{mV}[&F_{xf}\sin(\delta-\beta) + F_{yf}\cos(\delta-\beta) \\ &- F_{xr}\sin(\beta) + F_{yr}\cos(\beta)] - r\end{aligned} \tag{2}$$

$$\dot{r} = \frac{1}{I_{zz}}[a(F_{xf}\sin(\delta) + F_{yf}\cos(\delta)) - bF_{yr}] \tag{3}$$

where F_{xf}, F_{xr}, F_{yf} and F_{yr} represent the front and rear longitudinal and lateral forces, respectively, while r is the yaw rate, V the vehicle velocity, β the sideslip angle at the center of gravity (COG) of the vehicle, δ is the steering angle at the wheel and a and b are the distance between the front axle and the COG and the distance between the rear axle and the COG, respectively. Figure 1 shows a schematic representation of the vehicle model.
Lateral forces are modelled using the slip Fiala tire model [7] which, for a generic tire, reads:

$$\begin{cases} F_y = C_\alpha \tan\alpha - \dfrac{C_\alpha^2}{3F_{y,\max}}|\tan\alpha|\tan\alpha \\ \qquad\quad + \dfrac{C_\alpha^3}{27F_{y,\max}^2}\tan^3\alpha & |\alpha| \le \alpha_s \\ F_y = F_{y,\max}\mathrm{sgn}(\alpha) & \text{otherwise} \end{cases} \tag{4}$$

where C_α is the axle cornering stiffness (the sum of the two tires) and $F_{y,\max}$ is the maximum available axle lateral force, calculated using the friction circle theory:

$$F_{y,\max} = \sqrt{(\mu F_z)^2 - F_x^2} \tag{5}$$

where F_z is the vertical load and μ the friction coefficient.

Kinematic equations define front and rear tire slip angles:

$$\alpha_f = \delta - \arctan\left(\frac{V\sin\beta + ar}{V\cos\beta}\right) \tag{6}$$

$$\alpha_r = -\arctan\left(\frac{V\sin\beta - br}{V\cos\beta}\right) \tag{7}$$

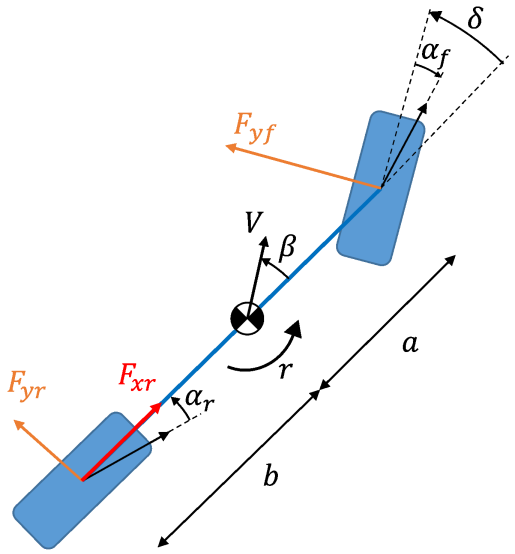

Figure 1: Schematic representation of the single track model adopted in the paper. α_f and α_r are the front and rear tire slip angles.

while α_s is the maximum slip angle beyond which the tire starts to slide

$$\alpha_s = \arctan\left(\frac{3F_{y,max}}{C_\alpha}\right) \tag{8}$$

The main vehicle and tires parameters used in this work are listed in Tab. 1. They resemble the dataset of an FSAE vehicle.

Table 1: Main vehicle and tire parameters.

Parameter	Symbol	Value
Mass	m	284 kg
Yaw moment of inertia	I_{zz}	109 kg m^2
COG to front axle distance	a	0.769 m
COG to rear axle distance	b	0.766 m
Front cornering stiffness	$C_{\alpha f}$	72 kN/rad
Rear cornering stiffness	$C_{\alpha r}$	72 kN/rad
Tire-road friction coefficient	μ	1

DEFINITION OF DRIFT

Several papers deal with drift analysis and definition. Drift, or power-slide [13], may be described as a particular cornering condition of the vehicle characterised by high sideslip angle, i.e., resulting in a significant mismatch between the direction the vehicle is pointing and the direction its centre of gravity is moving. Drift is typically associated with countersteer [14] - i.e., steering angle opposite to the direction of the turn - and rear axle saturation induced by a large rear drive torque [8].
In this work, we define drift as an unstable steady-state cornering motion with large rear tire slip angles, that are generally combined with countersteer. The condition of saturated rear tires is not strictly necessary for negotiating a turn while drifting. Nevertheless, in drifting condition

Table 2: Summary of types of equilibrium points.

Category	Stability	Steering $sign(r)sign(\delta)$
Stable-normal turn	Stable	1
Unstable-normal turn	Unstable	1
Drifting	Unstable	-1

the rear tire is most of the time saturated. This comes from the fact that for conventional tire models, high tire slip angles are associated to saturated lateral tire forces. An example of application of drifting without rear tire saturation is given in the bottom pictures of Figure 2.

We also define normal turn a steady-state cornering motion with steering angle in phase with (i.e., with the same sign of) the yaw rate. Indeed, having the car turning in accordance with the steering wheel rotation is intuitively what a driver would expect in "normal" driving mode. Stability-wise, there are two options: i) a stable-normal turn, i.e. a conventional normal turn, typically with small rear tire slip angles; ii) an unstable-normal turn, normally at larger rear slip angles than a conventional normal turn. Table 2 summarizes the three types of equilibria

We should point out that a normal turn (stable or unstable) is not always feasible. The existence of such equilibria is strictly related to the well-known phenomenon of saddle-node bifurcation, that is the disappearance of both stable- and unstable-normal turn equilibria, due to an aggressive combination of steering angle and vehicle velocity [15].

EQUILIBRIUM ANALYSIS

The equations of motion (1), (2) and (3) are functions of vehicle states (V, β, r) and driver inputs (δ, F_{xr}, F_{xf}):

$$\begin{aligned} \dot{V} &= f_V(V, \beta, r, \delta, F_{xr}, F_{xf}) \\ \dot{\beta} &= f_\beta(V, \beta, r, \delta, F_{xr}, F_{xf}) \\ \dot{r} &= f_r(V, \beta, r, \delta, F_{xr}, F_{xf}) \end{aligned} \tag{9}$$

A possible approach to study equilibria would be imposing driver inputs and then computing the corresponding steady-state values of vehicle states. We deem more insightful to investigate the vehicle behavior with a given turn to negotiate (R). So, several β for a fixed cornering radius, R, are assumed and their feasibility is investigated by calculating the corresponding V, δ and F_{xr} necessary to perform the maneuver. This is possible since yaw rate in steady state can be expressed by $|r| = V/R$. The front longitudinal force F_{xf} is set to zero, since the possibility of using brakes is discarded and rolling resistance can be neglected. Consequently, equations (9) are solved for fixed

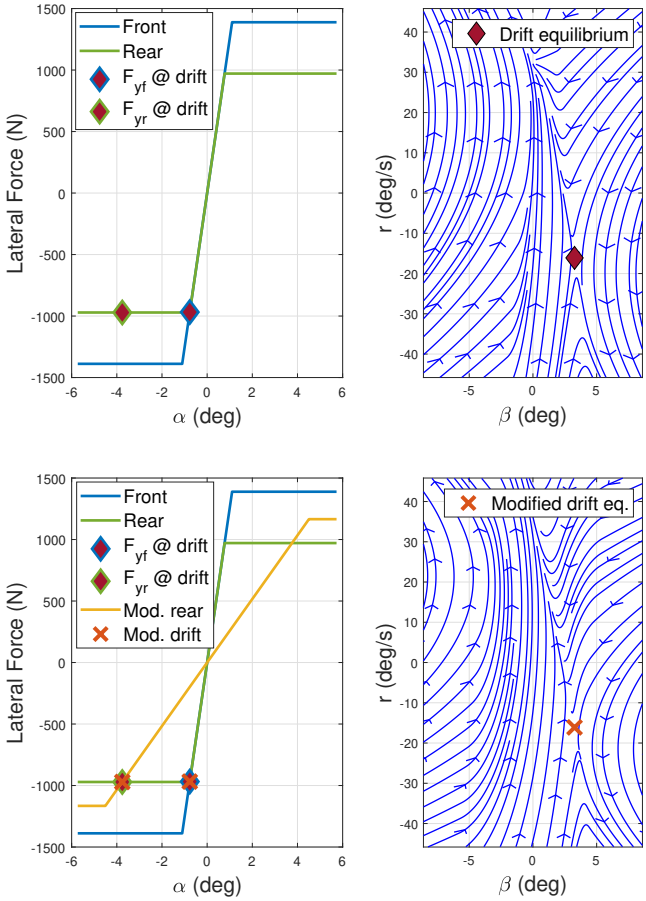

Figure 2: Drift equilibrium for a single-track model with bilinear tire model, $V = 25\,\mathrm{m/s}$, $\delta = 2°$, $F_{xr} = 1000\,\mathrm{N}$: lateral forces (left) and resulting phase plane (right). Top: cornering stiffness values from Table 1. Bottom: rear axle characteristic modified to have the same drift equilibrium but without saturating rear lateral force.

$\overline{\beta}$ and $\overline{R}$ in steady state

$$\begin{aligned} 0 &= f_V(V, \overline{\beta}, \overline{R}, \delta, F_{xr}) \\ 0 &= f_\beta(V, \overline{\beta}, \overline{R}, \delta, F_{xr}) \\ 0 &= f_r(V, \overline{\beta}, \overline{R}, \delta, F_{xr}) \end{aligned} \tag{10}$$

Two cornering radii are investigated, 20 and 40 m, while β varies between $-30°$ and $0°$. Driver inputs required to negotiate the given turn are computed at every step. The procedure is repeated for negative r to account for both cornering directions. Results for positive values of r (i.e., left turn) are shown in Figure 3 and 4.
Interestingly, in both scenarios the maximum velocity is reached in an unstable-normal turn, with a sideslip angle β_{Vmax} of about -1° and -2°, respectively. At the same time, the window of β values allowing for an unstable-normal turn shrinks when the cornering radius increases - (for R =20 m the range of β is between -0.5 and -4.8 deg, tightening between -1.4 and -3.8 deg for R =40 m. For the $R = 20$ m case, the top speed reachable with a stable-normal turn is more than for drifting conditions, the other way around happens when R is 40 m. Steering angle mag-

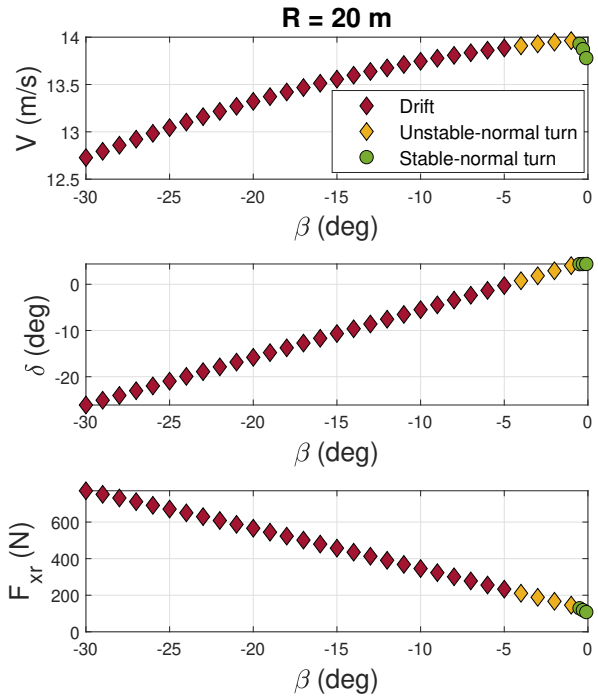

Figure 3: Vehicle speed (top), steering angle at the wheel (middle) and rear longitudinal force (bottom) for performing a turn of 20 m of cornering radius at different sideslip angles.

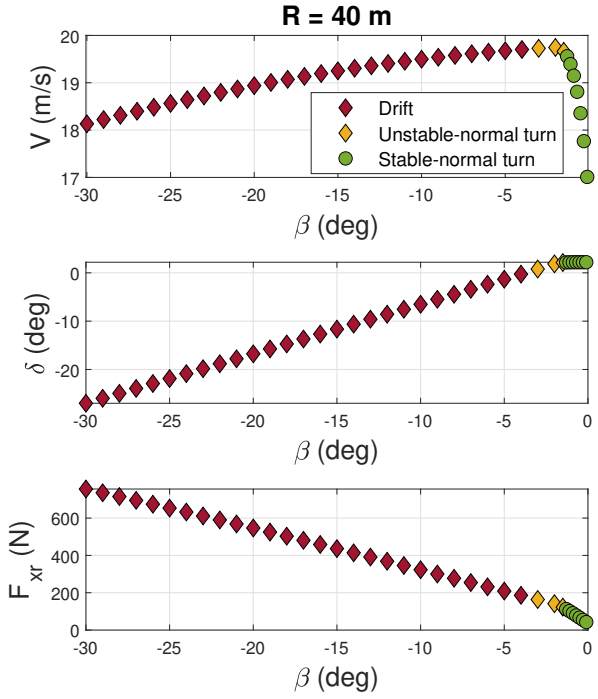

Figure 4: Vehicle speed (top), steering angle at the wheel (middle) and rear longitudinal force (bottom) for performing a turn of 40 m of cornering radius at different sideslip angles.

nitude and rear longitudinal force increase with sideslip angle magnitude, meaning that larger traction forces and counter steering angles are needed to sustain aggressive drifting conditions. Finally, negotiating the same turn with very high sideslip angles is never convenient in terms of travelling speed, since in both cases maximum velocities are obtained for $|\beta| < 5$ deg. On the other hand, $|\beta_{Vmax}|$ increases with R.

STABILITY ANALYSIS

Linearizing the system about equilibria allows to obtain a linear model able to describe the vehicle dynamics with sufficient accuracy [7]. Basically, the system is described by resorting to a linear state-space model representation:

$$\dot{\mathbf{x}} = \mathrm{A}\mathbf{x} + \mathrm{B}\mathbf{u} \tag{11}$$

where $\mathbf{x} = [V\ \beta\ r]^T$ is the state vector, $\mathbf{u} = [\delta\ F_{xr}]^T$ is the input vector, A is the state matrix and B is the input matrix. A and B are computed as the Jacobian matrices of the system with respect to the state vector and the input vector, respectively:

$$\mathrm{A} = \begin{bmatrix} \frac{\partial f_V}{\partial V} & \frac{\partial f_V}{\partial \beta} & \frac{\partial f_V}{\partial r} \\ \frac{\partial f_\beta}{\partial V} & \frac{\partial f_\beta}{\partial \beta} & \frac{\partial f_\beta}{\partial r} \\ \frac{\partial f_r}{\partial V} & \frac{\partial f_r}{\partial \beta} & \frac{\partial f_r}{\partial r} \end{bmatrix} \qquad \mathrm{B} = \begin{bmatrix} \frac{\partial f_V}{\partial \delta} & \frac{\partial f_V}{\partial F_{xr}} \\ \frac{\partial f_\beta}{\partial \delta} & \frac{\partial f_\beta}{\partial F_{xr}} \\ \frac{\partial f_r}{\partial \delta} & \frac{\partial f_r}{\partial F_{xr}} \end{bmatrix} \tag{12}$$

This linear representation allows to investigate stability by evaluating eigenvalues and eigenvectors of A. Eigenvectors identify the three main directions of convergence or divergence of trajectories near the point of linearization. The sign of the real part of the eigenvalues define whether the related direction is stable (negative real part) or not (positive real part). Fig. 5 presents several equilibrium points (circle and diamond) and the associated eigenvectors (arrows), for a cornering radius of 20 m. As expected, drift and unstable-normal turn points are actually saddle equilibria, i.e. they are characterised by one stable and two unstable eigenvalues. The stable equilibrium, instead, has only stable eigenvectors. Notice that the eigenvectors associated to the equilibria shown in Fig. 5 are not complex. It is possible to have equilibria characterised by complex conjugate eigenvalues and eigenvectors, but in this study such equilibria are restricted to a relatively limited range of β (approximately between -0.7 and -0.25 for $R = 20\,m$ and between -1.6 and -1.2 for $R = 40\,m$) - the identification of the main directions of convergence/divergence is physically meaningful only for real (non-complex) eigenvectors.

Figure 6 shows the (real part of) the eigenvalues of the system, for different sideslip angles. The drift equilibrium features the lowest real part of the stable eigenvalue, but the highest real part of one of the two unstable eigenvalues. The real part of the other unstable eigenvalue is nearly zero. The presence of complex conjugate eigenvalues may

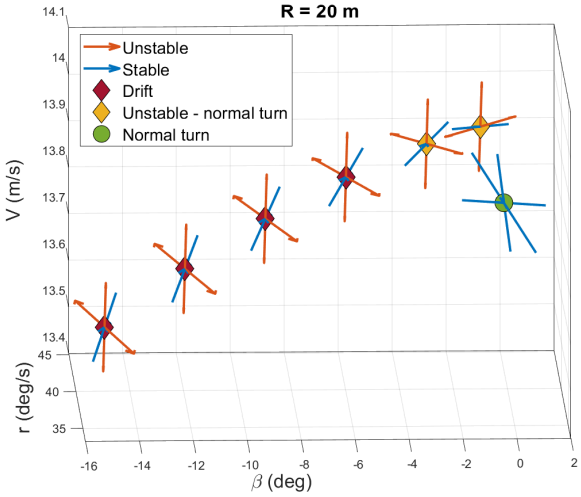

Figure 5: Comparison between eigenvectors for a 20 m radius turn in three cases: drift (red), unstable-normal turn (yellow) and stable-normal turn (green). Orange vectors are related to unstable eigenvalues, blue vectors are related to stable eigenvalues.

be spotted since two eigenvalues share the same real part for certain values of sideslip angle: a close-up of these eigenvalues is shown in Figure 7. Note that the eigenvalue that remains stable in all three scenarios (stable-normal, unstable-normal turn and drift) is never complex.

Looking back at the equations of motion, it is clear that equations (2) and (3) may be solved for β and r independently of equation (1), if V, F_{xr} and δ are considered as inputs. This means a two-dimensional (2D) system of differential equations may be solved at every vehicle speed V (with corresponding F_{xr} and δ from the three-dimensional system). The 2D system may be linearized and written as in (11), with state and input matrices being 2x2 submatrices of (12):

$$\mathrm{A} = \begin{bmatrix} \frac{\partial f_\beta}{\partial \beta} & \frac{\partial f_\beta}{\partial r} \\ \frac{\partial f_r}{\partial \beta} & \frac{\partial f_r}{\partial r} \end{bmatrix} \qquad \mathrm{B} = \begin{bmatrix} \frac{\partial f_\beta}{\partial \delta} & \frac{\partial f_\beta}{\partial F_{xr}} \\ \frac{\partial f_r}{\partial \delta} & \frac{\partial f_r}{\partial F_{xr}} \end{bmatrix}. \qquad (13)$$

Again, eigenvalues and eigenvectors of the state matrix give information about the stability of equilibria in the β–r plane. The equilibria shown in Figure 5 and their eigenvectors can be projected onto a β–r phase plane to better visualize the nature of the equilibrium points (see Figure 8, where three sample points are considered). Notice that $\beta-$ and $r-$ coordinates of equilibria computed in the 3D environment precisely identify also the position of equilibria of the 2D system when V is the equilibrium value [16]. The choice of reference system is such that the projection of two eigenvectors in the β–r plane give a very precise approximation of the eigenvectors resulting directly by the two-dimensional system, while one eigenvector is not visible, since its main component is in the V-axis. However, this result is not to be expected in general. If, for instance, longitudinal

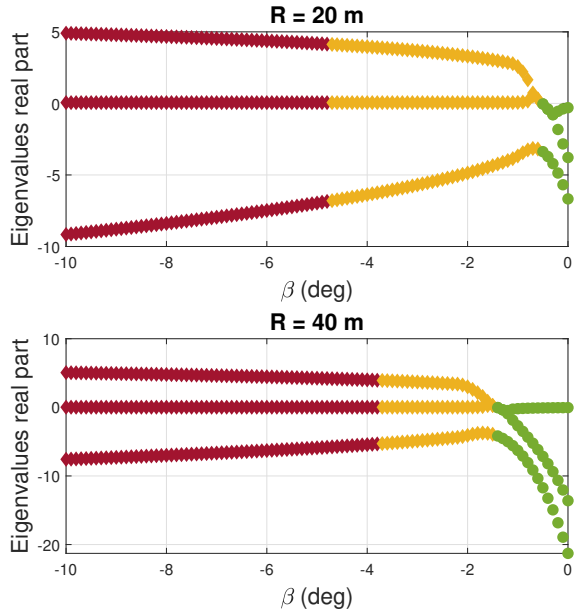

Figure 6: Real part of the eigenvalues of the system, for different sideslip angles and $R = 20\,m$ (top) and $R = 40\,m$ (bottom).

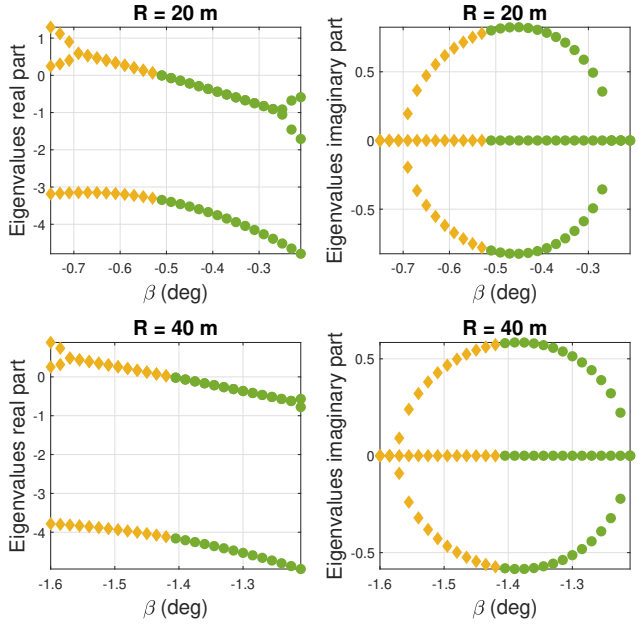

Figure 7: Close-up of the complex conjugate eigenvalues of the system. Real and imaginary parts are shown for $R = 20\,m$ (top) and $R = 40\,m$ (bottom).

and lateral velocities $u = V\cos(\beta)$ and $v = V\sin(\beta)$ were considered as independent variables instead of V and β, the projections of 3D eigenvectors in the $v-r$ plane would have considerably different directions with respect to 2D eigenvectors, computed at a given value of u.

The condition of an unstable-normal turn is further inves-

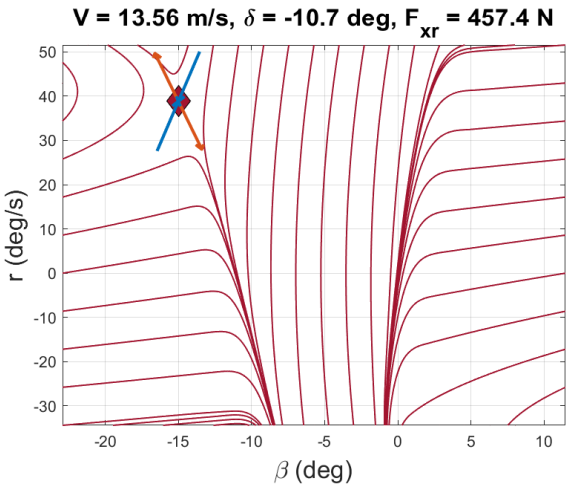

(a)

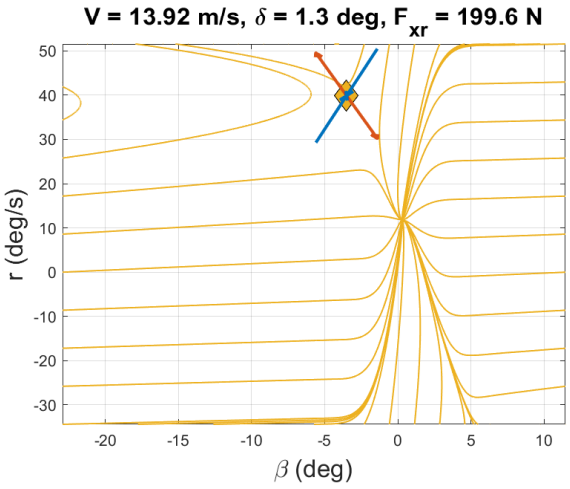

(b)

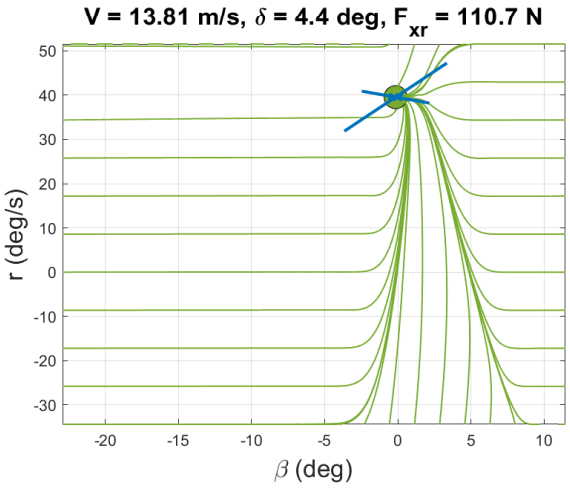

(c)

Figure 8: Two-dimensional $\beta - r$ phase plane in a. drifting condition b. unstable-normal turn and c. stable-normal turn. Three-dimensional eigenvectors are projected onto the $\beta - r$ plane, $R = 20\,m$.

tigated, since it is usually ignored in most of the literature dealing with steady-state cornering. The dynamic evolution of vehicle states in the neighborhood of the maximum speed condition for $R = 20$ m is considered. For this purpose, vehicle speed is let free to vary, hence the time evolution of the state can be represented in a three-dimensional phase space, where the state variables are β, r and V. In the considered framework, equilibrium curves can be identified, corresponding to the loci of the equilibrium points of the two-dimensional framework defined by only equations (2) and (3) [16]. Figure 9 presents the phase spaces obtained for the driver inputs computed above, at R=20 m and β =-1,-0.8,-0.6 and -0.4°. The corresponding $\beta - r$ phase plane is also shown at the vehicle velocity of equilibrium of the three-dimensional framework.

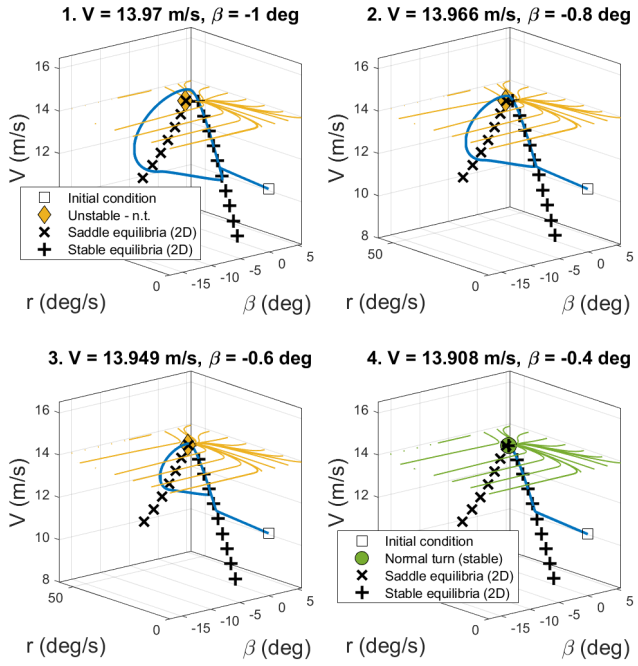

Figure 9: Three-dimensional phase space close to maximum speed (top-left). Diagrams 1 to 3 are characterised by a limit cycle, while in diagram 4 an asymptotically stable node is present. R is fixed at 20 m.

Interestingly, the time evolution of vehicle state is characterised by a stable limit cycle dynamic when the turn is performed the unstable-normal way. In this situation, an asymptotically stable equilibrium does not exists if V is not fixed, but only simple stability is possible. Hence an important remark is that these limit cycles are detectable only by including longitudinal dynamics.

ANALYTICAL EXPRESSION OF STATE MATRIX

In the previous section we showed that the state matrix of the linearized system is a useful tool for studying the stability of equilibria and, in general, gain insight on the system dynamics. Complex tire models may heavily affect the easiness of implementation of such linearized state matrix, making it difficult to obtain an analytical solution valid in the entire domain and not just locally (close to the linearization point). To solve this issue, a simplified

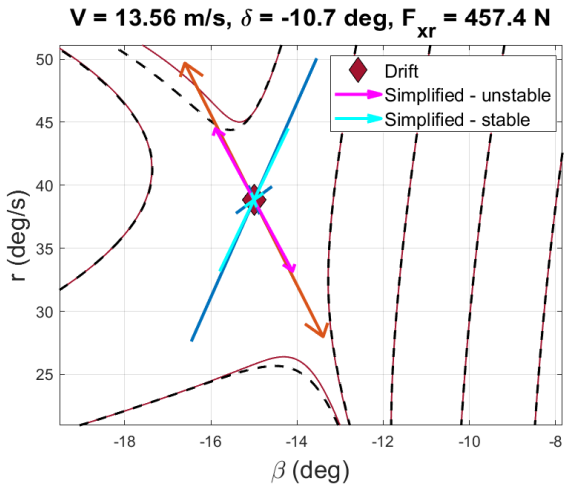

(a)

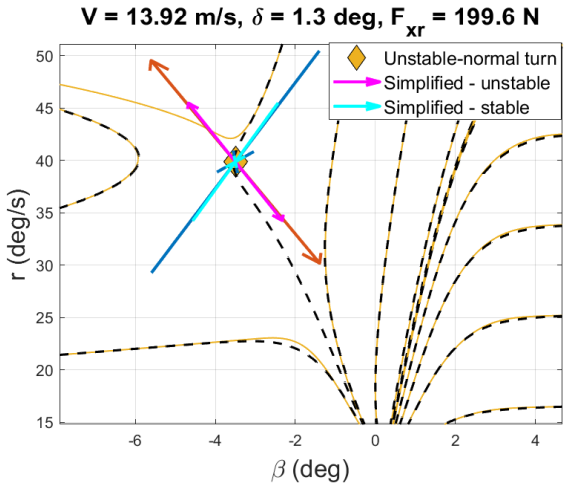

(b)

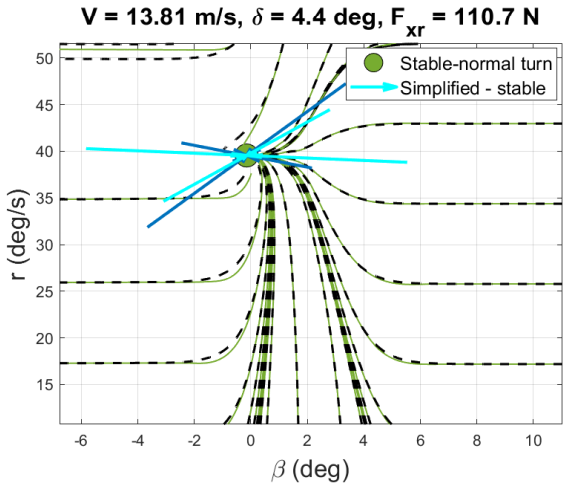

(c)

Figure 10: Comparison between baseline and simplified model with lateral forces modelled with hyperbolic tangent function in the neighborhood of a. drift equilibrium, b. unstable - normal turn equilibrium and c. stable equilibrium. Black-dotted curves represent the trajectories computed with the simplified model.

non-piecewise tire model is herein proposed, able to allow for a compact analytical solution, yet retaining the tire saturating pattern typical of a real tire model:

$$F_y = F_{y,max} \tanh\left(\frac{k\pi}{\alpha_{sl}}\alpha\right) \tag{14}$$

where $F_{y,\max}$ and α_s are defined according to (5) and (8), respectively, and the parameter k is selected to fit the Fiala tire model in (4). This formulation is able to capture in a single closed-form expression the two operating modes of the tire: i) linear region (for small α) and ii) saturated operation (for large α). This formulation simplifies the analytical analysis of the vehicle cornering motion when compared to the piecewise structure of the Fiala model. Moreover, it is continuous and differentiable in the whole domain. The analytical expression of the resulting linearized state matrix is:

$$\hat{\mathrm{A}} = \begin{bmatrix} \hat{\mathrm{a}}_{11} & \hat{\mathrm{a}}_{12} \\ \hat{\mathrm{a}}_{21} & \hat{\mathrm{a}}_{22} \end{bmatrix} \tag{15}$$

$$\begin{aligned}\hat{\mathrm{a}}_{11} = -\Bigg(& F_{xr}\cos\beta + c_5\sin(\beta-\delta)c_1 + c_2\sin\beta\cdot c_{13} \\ & + k\frac{\pi\cos\beta\cdot c_6 c_{13}(c_2^2-1)}{c_8 c_3} \\ & - k\frac{\pi\cos(\beta-\delta)(c_5^2-1)c_7 c_1}{c_{10}c_9}\Bigg)\frac{1}{mV}\end{aligned}$$

$$\begin{aligned}\hat{\mathrm{a}}_{12} = -\Bigg(& -\frac{a\pi\cos(\beta-\delta)(c_5^2-1)c_1}{c_4} \\ & + \frac{b\pi c_{13}(c_2^2-1)}{V c_8 c_3}\Bigg)\frac{k}{mV} - 1\end{aligned}$$

$$\hat{\mathrm{a}}_{21} = -\left(\frac{a\pi\cos\delta\cdot(c_5^2-1)c_7c_1}{c_{10}c_9} + \frac{b\pi c_6 c_{13}(c_2^2-1)}{c_8 c_3}\right)\frac{k}{J}$$

$$\hat{\mathrm{a}}_{22} = -\left(\frac{a^2\pi\cos\delta\cdot(c_5^2-1)c_1}{c_4} + \frac{b^2\pi c_{13}(c_2^2-1}{V\cos\beta\cdot c_8 c_3}\right)\frac{k}{J}$$

where

$$
\begin{aligned}
c_1 &= \sqrt{\mu^2 F_{zf}^2} \\
c_2 &= \tanh\left(k \frac{\pi \arctan\left(\frac{c_{11}}{V\cos\beta}\right)}{c_8}\right) \\
c_3 &= \frac{c_{11}^2}{c_{15}} + 1 \\
c_4 &= V\cos\beta \cdot c_{10} c_9 \\
c_5 &= \tanh\left[k \frac{\pi\left(\delta - \arctan\left(\frac{c_{14}}{V\cos\beta}\right)\right)}{c_{10}}\right] \\
c_6 &= \frac{\sin\beta \cdot c_{11}}{c_{12}} - 1 \\
c_7 &= \frac{\sin\beta \cdot c_{14}}{c_{12}} + 1 \\
c_8 &= \arctan\left(\frac{3c_{13}}{C_{yr}}\right) \\
c_9 &= \frac{c_{14}^2}{c_{15}} + 1 \\
c_{10} &= \arctan\left(\frac{3\mu F_{zf}}{C_{yf}}\right) \\
c_{11} &= br - V\sin\beta \\
c_{12} &= V\cos^2\beta \\
c_{13} &= \sqrt{\mu^2 F_{zr}^2 - F_{xr}^2} \\
c_{14} &= ar + V\sin\beta \\
c_{15} &= V^2\cos^2\beta \\
k &= 0.86
\end{aligned}
$$

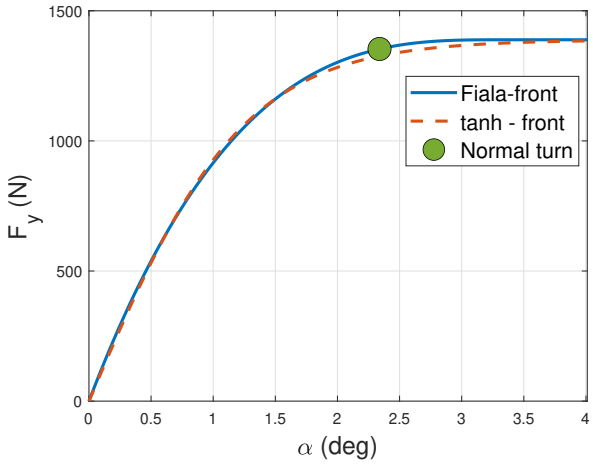

Figure 11: Comparison between tire side force characteristic computed with Fiala and hyperbolic tangent model. Only the front axle is presented for visualization purposes.

The analytical expression of the state matrix remains comprehensible and accessible, but at the same time this simplified model allows to obtain results comparable to the ones of the baseline model. The $\beta - r$ phase planes presented in Figure 8 are compared to phase planes defined modelling the tire lateral forces using (14). A close-up in the neighborhood of equilibrium is shown in Figure 10. Eigenvectors are almost perfectly aligned to the ones computed using the original model for saddle nodes, while the directions of convergence are slightly different in the third case (stable node). Observe that the condition of stable-normal turn considered so far, even if stable, is close to saddle-bifurcation. This means tires are working in the transition region, between the linear and the saturated parts of the Fiala model (see Figure 11), which is where there Fiala and simplified model exhibit the maximum deviation.

CONCLUSIONS

This paper provided a systematic analysis of the steady-state and dynamic cornering motion of vehicles. The analysis of cornering motion was divided into three main categories (stable-normal turn, unstable-normal turn and drifting) and took into account stability and countersteering criteria. We found out that the "unstable-normal turn" provides the maximum vehicle velocity for a given radius of curvature. At the same time, the range of driver inputs generating this equilibrium is limited and reduces when increasing R. Phase portraits were employed to gain better understanding of the stability of the equilibrium points, revealing the existence of limit cycles in the (sideslip, yaw-rate, velocity) space. A compact lateral tire model was also proposed, which simplified the analytical analysis of the cornering vehicle motion. Future work shall include a more detailed study of the conditions for the existence of limit cycles in the vehicle cornering motion, and experimental validation.

ACKNOWLEDGEMENTS

This work was supported in part by the Italian Ministry of Foreign Affairs and International Cooperation, grant number PGR01170.

REFERENCES

[1] Peide Cai, Xiaodong Mei, Lei Tai, Yuxiang Sun, and Ming Liu. High-speed autonomous drifting with deep reinforcement learning. IEEE Robotics and Automation Letters, 5(2):1247–1254, 2020.

[2] Rami Y Hindiyeh and J Christian Gerdes. Equilibrium analysis of drifting vehicles for control design. In Dynamic Systems and Control Conference, volume 48920, pages 181–188, 2009.

[3] Efstathios Velenis, Emilio Frazzoli, and Panagiotis Tsiotras. On steady-state cornering equilibria for wheeled vehicles with drift. In Proceedings of the 48h IEEE Conference on Decision and Control (CDC) held jointly with 2009 28th Chinese Control Conference, pages 3545–3550. IEEE, 2009.

[4] Christoph Voser, Rami Y Hindiyeh, and J Christian

Gerdes. Analysis and control of high sideslip manoeuvres. Vehicle System Dynamics, 48(S1):317–336, 2010.

[5] Carrie G Bobier-Tiu, Craig E Beal, John C Kegelman, Rami Y Hindiyeh, and J Christian Gerdes. Vehicle control synthesis using phase portraits of planar dynamics. Vehicle System Dynamics, 57(9):1318–1337, 2019.

[6] Jonathan Y Goh and J Christian Gerdes. Simultaneous stabilization and tracking of basic automobile drifting trajectories. In 2016 IEEE Intelligent Vehicles Symposium (IV), pages 597–602. IEEE, 2016.

[7] Marsie T Peterson, Tushar Goel, and J Christian Gerdes. Exploiting linear structure for precision control of highly nonlinear vehicle dynamics. IEEE Transactions on Intelligent Vehicles, 8(2):1852–1862, 2022.

[8] Michele Vignati, Edoardo Sabbioni, and Federico Cheli. A torque vectoring control for enhancing vehicle performance in drifting. Electronics, 7(12):394, 2018.

[9] Sina Milani, Hormoz Marzbani, and Reza N Jazar. Vehicle drifting dynamics: discovery of new equilibria. Vehicle system dynamics, 60(6):1933–1958, 2022.

[10] M. Guiggiani. The Science of Vehicle Dynamics. Springer, 2014.

[11] Rami Yusef Hindiyeh. Dynamics and control of drifting in automobiles. PhD thesis, Stanford University, 2013.

[12] Tushar Goel, Jonathan Y Goh, and J Christian Gerdes. Opening new dimensions: Vehicle motion planning and control using brakes while drifting. In 2020 IEEE Intelligent Vehicles Symposium (IV), pages 560–565. IEEE, 2020.

[13] Johannes Edelmann and Manfred Plöchl. Handling characteristics and stability of the steady-state powerslide motion of an automobile. Regular and Chaotic Dynamics, 14:682–692, 2009.

[14] Johannes Edelmann, Manfred Plöchl, and Peter Pfeffer. Analysis of steady-state vehicle handling and driver behaviour at extreme driving conditions. na, 2011.

[15] Eiichi Ono, Shigeyuki Hosoe, Hoang D Tuan, and Shun'ichi Doi. Bifurcation in vehicle dynamics and robust front wheel steering control. IEEE transactions on control systems technology, 6(3):412–420, 1998.

[16] Craig E Beal and Christina Boyd. Coupled lateral-longitudinal vehicle dynamics and control design with three-dimensional state portraits. Vehicle System Dynamics, 57(2):286–313, 2019.